4D Retrospective Black Blood TrueFISP Imaging of Mouse Heart

Sylvain Miraux,[1*] Guillaume Calmettes,[1] Philippe Massot,[1] William Lefrançois,[1] Elodie Parzy,[1] Bernard Muller,[2] Laurent M. Arsac,[1] Véronique Deschodt-Arsac,[1] Jean-Michel Franconi,[1] Philippe Diolez,[1] and Eric Thiaudière[1]

The purpose of this study was to demonstrate the feasibility of steady-state True fast imaging with steady precession (TrueFISP) four-dimensional imaging of mouse heart at high resolution and its efficiency for cardiac volumetry. Three-dimensional cine-imaging of control and hypoxic mice was carried out at 4.7 T without magnetization preparation or ECG-triggering. The *k*-space lines were acquired with the TrueFISP sequence (pulse repetition time/echo time = 4/2 ms) in a repeated sequential manner. Retrospective reordering of raw data allowed the reconstruction of 10 three-dimensional images per cardiac cycle. The acquisition scheme used an alternating radiofrequency phase and sum-of-square reconstruction method. Black-blood three-dimensional images at around 200 μm resolution were produced without banding artifact throughout the cardiac cycle. High contrast to noise made it possible to estimate cavity volumes during diastole and systole. Right and left ventricular stroke volume was significantly higher in hypoxic mice vs controls (20.2 ± 2 vs 15.1 ± 2; $P < 0.05$, 24.9 ± 2 vs 20.4 ± 2; $P < 0.05$, respectively). In conclusion, four-dimensional black-blood TrueFISP imaging in living mice is a method of choice to investigate cardiac abnormalities in mouse models. Magn Reson Med 62:000–000, 2009. © 2009 Wiley-Liss, Inc.

Key words: TrueFISP; black blood; retrospective gating; mouse heart; cine-3D

Owing to the many possibilities offered by transgenic and surgical approaches, numerous models of cardiovascular diseases have been developed in mouse. This provides not only a better understanding of physiology but is also of great use in preclinical trials, e.g., gene therapy or pharmacological treatment.

MRI has become a reference noninvasive tool to characterize variations in structure and function of mouse heart. Until now, most of the MR studies on mouse models were performed with two-dimensional white-blood cine-imaging combined with cardiac triggering for MR acquisition synchronization (1-4). Parameters like end-systolic and end-diastolic volumes can be measured in order to evaluate both stroke volume and ejection fraction. Nevertheless, routine MRI techniques suffer from many drawbacks. First of all, two-dimensional imaging results in a limited spatial resolution in the slice dimension. In fact, typical out-of-plane resolutions are in the range of 1 mm, whereas mouse heart does not exceed 10 mm in the long axis. This could result in measurement errors due to a partial volume effect.

To overcome this issue, some authors have shown interest in performing four-dimensional (4D) (three-dimensional [3D]-cine) imaging (5-7). Feintuch et al. (6) demonstrated the feasibility of 4D mouse imaging with an isotropic spatial resolution of 200 μm. Nevertheless, scan times were very long (between 80 and 120 min) for bright blood imaging. More recently, Bucholz et al. (7) presented impressive images with exceptional resolution (80 μm), but injection of a nonconventional liposomal gadolinium contrast agent was required. The other drawback of such experiments is that, in many cases, images are acquired with a bright blood contrast. It is now widely accepted that MR sequences with suppression of the blood signal (black or dark blood sequence) are more appropriate to reduce interobserver variability in the drawing of epicardial and endocardial borders (8), and consequently allow more accurate estimation of the physiologic parameters of the heart. Among the many black-blood imaging methods that have been developed in mouse models and in humans (9-13), most of them required the implementation of a preparation module (spatial presaturation, motion sensitizing gradients, or double inversion recovery). However, magnetization preparation has some disadvantages, especially the need to increase the pulse repetition time (TR) of the sequence. Moreover, this makes it difficult to use fast steady-state free precession, particularly on small animal models when the duration between two R-waves is lower than 200 ms.

Steady-state free precession–based imaging (14), particularly TrueFISP (also called balanced steady state free precession (bSSFP) or fast imaging employing steady state acquisition (FIESTA), can play a key role in clinical heart imaging (15) because of high signal-to-noise and contrast-to-noise ratios. Nowadays, they are even used in 4D white-blood imaging in humans, where a complete cardiac cycle can be acquired in a single breath hold (16-18). Unfortunately, the TrueFISP sequence is very sensitive to local field variations, resulting in characteristic banding artifacts. This explains why it is seldom employed at high field, particularly on small animals. However, by combining an alternating radiofrequency (RF) phase method and sum-of-square reconstruction (19,20), it has recently been shown that high-resolution 3D images can be viewed at 4.7 T and 9.4 T in mouse brain, with high contrast and with a much reduced scan time compared to a rapid acquisition with relaxation enhancement (RARE) 3D sequence (20).

[1]Centre de Résonance Magnétique des Systèmes biologiques, UMR 5536 CNRS/Université Victor Segalen Bordeaux 2, Bordeaux, France

[2]Laboratoire de Pharmacologie de l'UFR Pharmacie, Institut National de la Santé et de la Recherche Médicale U885, Université Victor Segalen Bordeaux 2, Bordeaux, France

*Correspondence to: Sylvain Miraux, CNRS/UVSB2, 146, rue Leo Saignat, Bordeaux, 33076, France. E-mail: miraux@rmsb.u-bordeaux2.fr

Received 4 February 2009; revised 18 June 2009; accepted 19 June 2009.

DOI 10.1002/mrm.22139

Published online in Wiley InterScience (www.interscience.wiley.com).

The goal of this study was to perform TrueFISP (alternating RF pulse phase with sum-of-square reconstruction) in order to acquire black-blood 3D cine images of mouse heart. Images without ECG triggering were acquired at 4.7 T with retrospective rearrangement. The method was employed to accurately define cardiovascular anatomy and function of control mice and to describe changes induced by exposure to chronic hypoxia.

MATERIALS AND METHODS

Magnet and Gradient System

Experiments were carried out on a horizontal 4.7-T Biospec system (Bruker, Ettingen, Germany). The system was equipped with a 6-cm gradient insert capable of 950 mT/m maximum strength and 80 μs rise time. Measurements were performed with a mouse-dedicated birdcage cross-polarization resonator, 25 mm in diameter and 60 mm long, tuned to 200.3 MHz.

Animal Preparation

Female mice (C57 black 6, mean body weight = 20 ± 0.6 g) were separated into two groups. One group (chronic hypoxia) was exposed to a simulated altitude of 5500 m (barometric pressure 380 mmHg) in a well-ventilated, temperature-controlled hypobaric chamber for 28 days. The chamber was opened briefly three times a week for household cleaning and feeding. The other group (normoxic mice, control) was maintained under ambient normoxic conditions, with the same 12:12-h light-dark cycles. Free access to a standard mouse diet and water was allowed throughout the exposure period (21). The investigation conformed to the National and European Research Council Guide for the care and use of laboratory animals.

For MRI investigation, mice were anesthetized with 1.5-2% isoflurane (Centravet, La Palisse, France) mixed in air. The ECG signal was picked up by electrodes placed on the forelimbs. When the R-wave was detected, a square pulse (2-ms duration) was generated by a dedicated monitoring system (SA Instruments, Inc., NY, USA) and recorded on a data acquisition system at a sampling frequency of 10 kHz (Powerlab, AD Instruments, Bella Vista, Australia).

Visualization of ECG via a user interface allowed cardiac rhythm stabilization (475-525 beats/min) by modifying the percentage of isoflurane.

The animals were positioned supine within the magnet, with the heart placed at the center of the NMR coil. The total experiment time for one mouse was approximately 75 min (10 min preparing, 5 min for MRI adjustments, and 60 min for 4D MRI).

MRI Parameters

Four sets of 48 sequential repetitions of nontriggered, nonselective, coronally orientated 3D TrueFISP were performed: echo time/TR = 2/4 ms: excitation pulse: hermite (410 μs), flip angle: 65°; field of view: 35 × 19 × 16 mm; matrix: 192 × 94 × 48; spatial resolution: 182 × 202 × 333 μm; reception bandwidth: 77,519 Hz (404 Hz/pixel).

Total acquisition time for one set was 14 min 26 sec.

As previously described (20), each data set was acquired with a specific difference in phase ($\Delta\Phi$) between consecutive RF pulses ($\Delta\Phi$ = 180°, 0°, 90°, 270°).

Each acquired line of the *k*-space was separately recorded for retrospective reconstruction of the cine images.

At each TR, a 410 μs TTL signal was generated by the spectrometer and recorded by the four-channel data acquisition system (Powerlab, AD Instruments).

Black-Blood Contrast

Black-blood contrast was obtained without any preparation module, thanks to whole-body imaging acquisition. Since the 3D imaging volume encompassed the RF excitation region, no time-of-flight effect was expected. High flip angle and short repetition time were used to achieve complete saturation of blood signal.

Retrospective 4D image reconstruction

Images (Fig. 1) were reconstructed with homemade software developed on Igor Pro (Wavemetrics, Lake Oswego, OR).

Each line (echo) of the *k*-space of 3D data sets was characterized by its $\Delta\Phi$, its phase-encoding gradient, its slice-encoding gradient, and its time delay following the R-wave peak, as monitored by the data acquisition system. The *k*-space lines were appropriately rearranged into 3D matrices, each of them having its $\Delta\Phi$ and its time delay with respect to the R-wave. Here, 10 time delays were defined throughout the cardiac cycle. For each time delay, four matrices corresponding to the four $\Delta\Phi$ values were recombined by the sum-of-square method after Fourier transformation.

About 30 echoes were acquired between two consecutive RR waves and 48 acquisitions of the 3D data sets were carried out. As the k-spaces lines were statistically filled, many lines were acquired several times and their signal was averaged accordingly. The probability of having empty lines in 3D matrices at a given time delay was less than 1%.

Volume Analysis

Volume analysis was performed with a semiautomated segmentation procedure on Amira (Visage Imaging GmbH, Germany) to calculate left ventricular end-diastolic volume, left ventricular end-systolic volume, left ventricular stroke volume, left ventricular ejection fraction, right ventricular end-diastolic volume, right ventricular end-systolic volume, right ventricular stroke volume, and right ventricular ejection fraction. Right ventricle and left ventricle + septum volumes were also assessed by MRI and compared to wet muscle mass, as assessed from excised heart dissection and weighting.

Steady-State Magnetization Simulations

Simulations of the state of magnetization with TrueFISP and gradient echo sequences using ERNST angle were performed with Igor Pro using well-known equations (see Appendix).

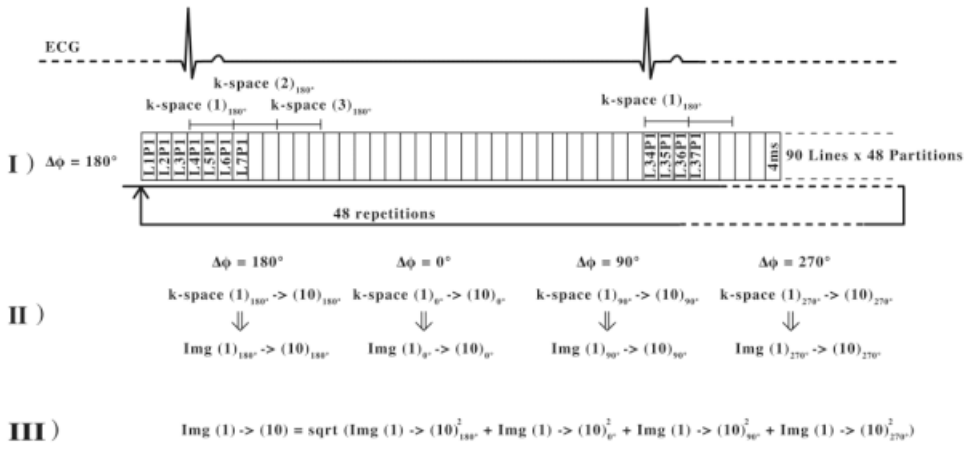

FIG. 1. Schematic diagram of acquisition and reconstruction of retrospective 3D cine TrueFISP cardiac imaging. **I:** 3D TrueFISP matrix was acquired 48 times for a given value of $\Delta\Phi$ (here 180°). The same protocol was repeated for $\Delta\Phi = 0°$, 90° and 270°. The *k*-spaces are denoted as LiPj, where L stands for the phase-encoding step and P the partition-encoding step. Here around 30 echoes were recorded during an R-R interval. **II:** The *k*-space data were rearranged as a function of time and averaged to build 10 3D matrices in one R-R interval for a given $\Delta\Phi$ value. The same rearrangement was carried out for the other values of $\Delta\Phi$. **III:** Sum-of-square reconstruction of the 10 images from each $\Delta\Phi$ value.

Statistical Analysis

Values are given as mean ± SD (*n*: number of animals). Cardiac parameters were compared by one-way analysis of variance. Statistical significance was considered for a *P* value lower than 0.05.

RESULTS

Black-blood 3D cine TrueFISP of the mouse heart was carried out at 4.7 T by using retrospective ECG-gating combined with the method of linear combination of alternating RF phase acquisitions and sum-of-square reconstruction.

Since the TrueFISP sequence is known to yield a high signal-to-noise ratio (SNR), particularly for tissue with long T_2, simulations of the steady-state magnetization obtained with TrueFISP for the myocardium were performed and compared to a classic gradient echo sequence. Simulations were performed for a tissue with $T_1 = 1300$ ms and $T_2 = 50$ ms. T_1 and T_2 values were selected from literature data (22,23).

As described in Fig. 2, simulations of the stationary state showed that at TR = 4 ms, the stationary state magnetization with TrueFISP was 1.47-fold higher compared to a gradient echo at the Ernst angle. Based on these simulations, therefore, TrueFISP with high flip angle was used for cardiac imaging.

Retrospective gating without ECG triggering of the pulse sequence was essential to maintain a stationary state during the whole experiment, a requisite of TrueFISP imaging. The ECG signal was recorded concomitantly with the NMR signal in order to assign the position of each acquired *k*-space line in the cardiac cycle.

First, the *k*-space volume (matrix: 192 × 94 × 48) was acquired 48 times, with a value $\Delta\Phi = 180°$. In general, the heart rate in both groups ranged from 475 to 525 beats/min, resulting in a $T_{R\text{-}R}$ = 115-125 ms. The TR of the sequence was equal to 4 ms and to improve the SNR, three successive lines were used to reconstruct the 3D image corresponding to a given time point. Therefore, the temporal resolution became 12 ms, thereby allowing the reconstruction of about 10 cine images.

Figure 3a and b shows two views (axial and coronal) of a 3D image at end systole, obtained with the value $\Delta\Phi$ = 180°. On these images, the blood signal appears completely suppressed in the ventricles and only the myocardium is visible. Subcutaneous fat appears hyperintense. Despite a high SNR (≈ 15), the poor magnetic field homogeneity induced a band of signal loss. This banding artifact prevented interpretation and estimation of the cardiac volume.

Therefore, three more sets of images were acquired with values of $\Delta\Phi = 0°$, 90°, 270° and were reconstructed with

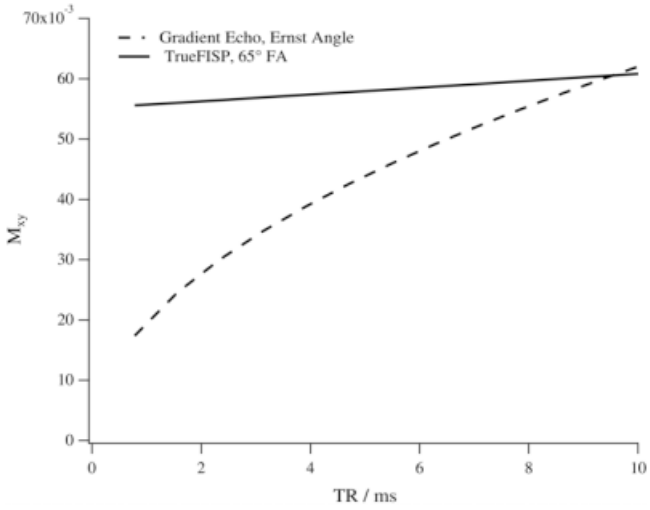

FIG. 2. Simulations of magnetization equilibrium state with TrueFISP (α = 65°) and gradient echo at the Ernst angle for a tissue with T_1 = 1300 ms and T_2 = 50 ms.

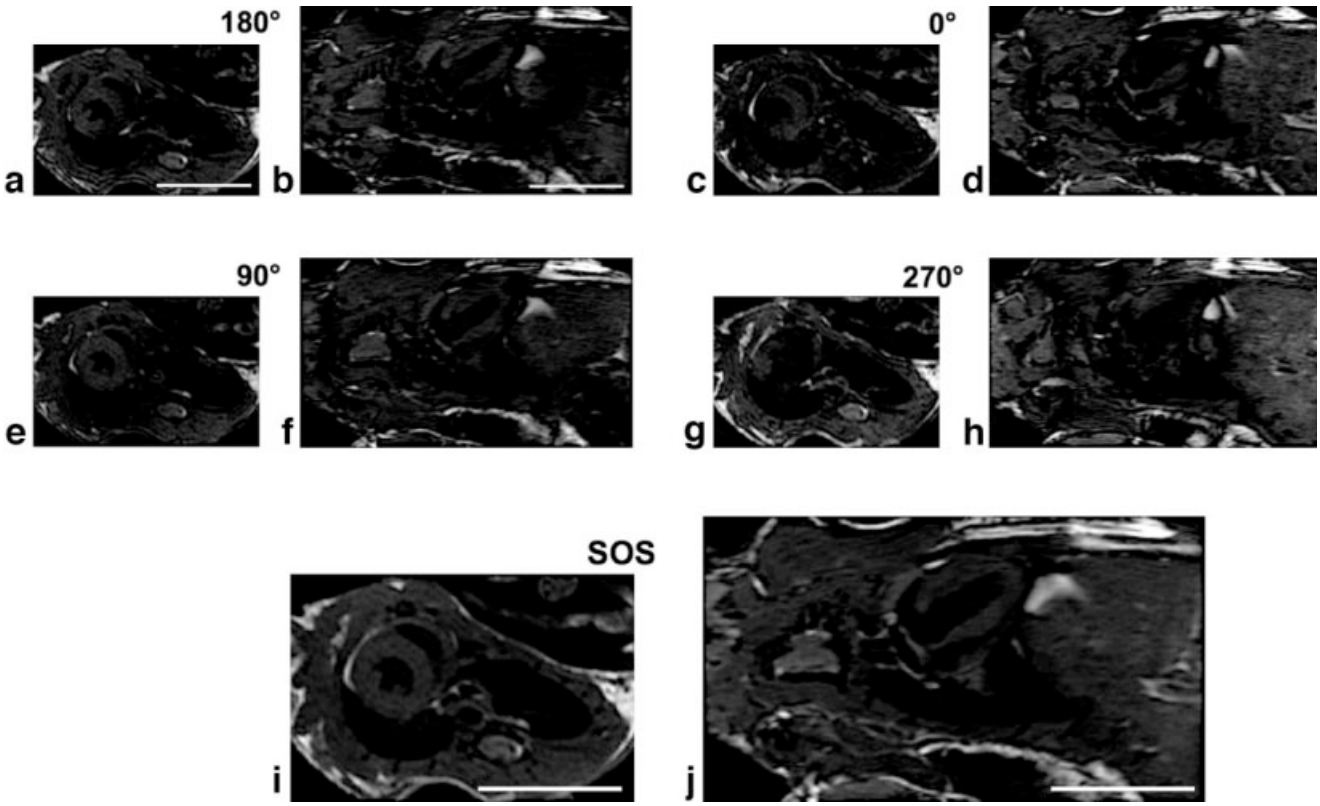

FIG. 3. Extracted views (axial and coronal) of 4D images obtained with TrueFISP $\Delta\Phi = 180°$ **(a,b)**, 0° **(c,d)**, 90° **(e,f)**, and 270° **(g,h)** and final views obtained after sum-of-square reconstruction **(i,j)**. Scale bars represent 1 cm.

the sum-of-square method. Images are shown in Fig. 3i,j. They appear artifact free and with a very good black-blood contrast. The SNR of the myocardium region was then around 26.

Figure 4 shows the series of 10 cardiac 3D cine images in two orientations (short and long axis). Image quality was constant (SNR of myocardium and blood suppression) throughout the cardiac cycle. Both ventricles were easily

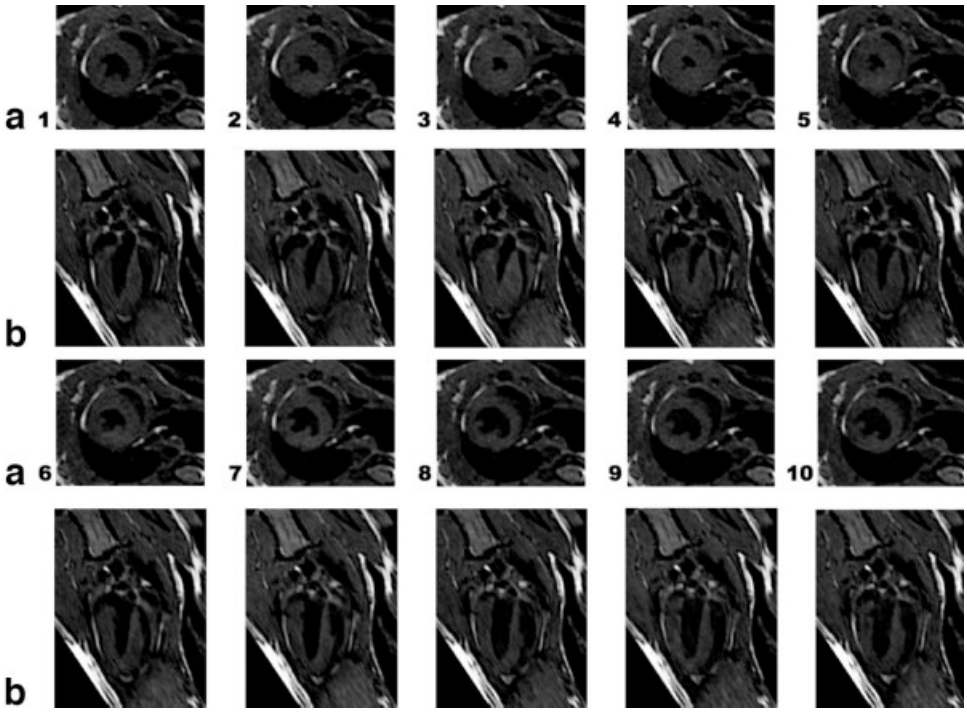

FIG. 4. Magnified short axis (line A) and long axis (line B) views from 3D images obtained after reconstruction of the 10 phases of the cardiac cycle of a normal mouse. Movies of normal mouse beating heart are available as supplementary materials.

Table 1
Quantitative Measurements of Left and Right Ventricles in Normal and Hypoxic Mice

	LVEDV (μL)	LVESV (μL)	LVSV (μL)	LVEF (%)	RVEDV (μL)	RVESV (μL)	RVSV (μL)	RVEF (%)
Normoxic mice ($n = 6$)	35 ± 3	10.1 ± 2	24.9 ± 2	71.1 ± 3	24.3 ± 2	9.2 ± 2	15.1 ± 2	62.1 ± 3
Chronic hypoxic ($n = 5$)	28.8 ± 3*	8.4 ± 2	20.4 ± 2*	70.8 ± 3	31.8 ± 2*	11.6 ± 2	20.2 ± 2*	63.5 ± 3

LVEDV, left ventricular end-diastolic volume; LVESV, left ventricular end-systolic volume; LVSV, left ventricular stroke volume; LVEF, left ventricular ejection fraction; RVEDV, right ventricular end-diastolic volume; RVESV, right ventricular end-systolic volume; RVSV, right ventricular stroke volume; RVEF, right ventricular ejection fraction. * $P < 0.05$ (analysis of variance test).

delineated, and their volume could be measured after semiautomated segmentation. The control values of end-diastolic, end-systolic, stroke volume, and ejection fraction of both ventricles given in Table 1 are in agreement with values already reported in the literature (6-8).

The same technique was applied on hypoxic mice ($n = 5$), an animal model developing the same cardiac changes as observed in humans during severe chronic obstructive pulmonary disease, hypoxemic congenital heart disease, or high-altitude living. Figure 5 shows images of a hypoxic mouse heart. The left ventricular cavity volume appears slightly decreased on the image, the right ventricle appears bigger during the end of systole, and the right ventricle wall (see arrow in Fig. 5b) seems thicker compared to that in control mice. The values in Table 1 show a significant difference in left ventricular end-diastolic volume, left ventricular stroke volume, right ventricular end-diastolic volume and right ventricular end-systolic volume.

Myocardium region could also be manually segmented, and volumes measured by MRI were compared to wet muscle mass of excised dissected hearts. The values are reported in Table 2 and show significant difference in right ventricle volume measured between control and hypoxic mice. This difference was confirmed from ex vivo weighing of dissected hearts.

A movie of normal mouse beating heart is available at http://www.rmsb.u-bordeaux2.fr/rmsb/Recherche/Pages-Perso/Sylvain/ImagFonc/Imagerie_4D_cardiaque.html.

DISCUSSION

High-resolution 3D cine black-blood cardiac imaging in living mice was carried out in the present study. In terms of spatial resolution, 3D imaging can bring a significant advantage over conventional two-dimensional imaging, especially in mouse heart that has an overall size of about 200 μL. In separate experiments (not shown) carried out on a 235-μL water phantom, it was shown that errors in volume measurements were lower (4%) in 3D imaging with a voxel size of $192 \times 200 \times 333$ (μm) (^{3}) than in two-dimensional images with pixel size of 100×100 (μm) (^{2}) and a slice thickness of 1 mm (9%). Thus, there is a strong interest in using nearly isotropic voxels in assessing the volume of tiny structures.

Here, the TrueFISP sequence was used at high field. Several key points are required to obtain such high-quality images. First of all, a coil irradiating most of the body (approximately 8 cm long) is necessary to suppress blood signal at the cardiac level and in vessels. In this study, the coil length was 6 cm and blood signal was efficiently saturated. By contrast, when the same acquisition parameters were used with a 30-mm-long coil, the blood appeared hyperintense in some areas of the heart ventricles. This is due to the time-of-flight effect generated by the RF gradient of the small coil.

To limit the time-of-flight effect, the slice thickness should encompass the whole animal. Of course, this kind of 3D "whole-body" acquisition requires a large matrix size in the third dimension to conserve a high spatial resolution and consequently increases the total scan time. An advantage, however, is that no particular slice positioning is required and that images in different orientations (long and short axis) can be reconstructed a posteriori.

The last reason for a good black-blood contrast was the use of a short TR and a high flip angle (65°). Blood is characterized by a long T_1 compared to other tissues and was thus well saturated. The main advantage of the technique is that no preparation is necessary to cancel blood magnetization.

A much-debated issue about using gradient echo sequences with short TR and a high flip angle is the low stationary state magnetization achieved, thus limiting the SNR. For this reason, TrueFISP acquisition was preferred to FLASH or FISP sequences. As shown in Fig. 2, TrueFISP makes it possible to obtain a stationary state magnetization 1.5-fold higher than with a FLASH sequence at the Ernst angle (and 10-fold higher with a FLASH sequence at 65°

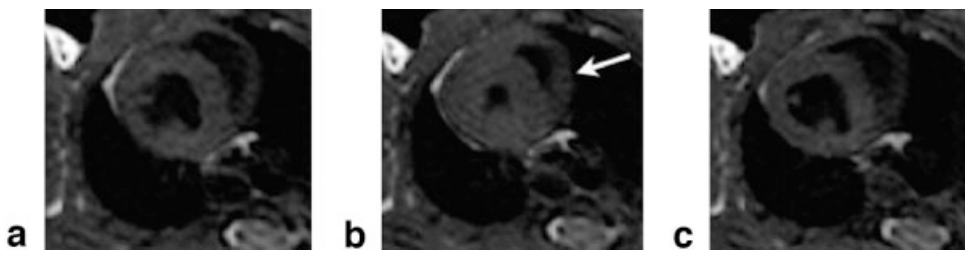

FIG. 5. Three extracted short axis views of a hypoxic mouse heart (end diastole **(a)**, end systole **(b)**). Arrows show wall thickness enhancement clearly visible compared to that of control mouse.

Table 2
Right Ventricle and Left Ventricle + Septum Volumes Measured With MRI (in μl) and Corresponding Wet Muscle Masses (in mg) of Excised Hearts From Normal and Hypoxic Mice

	MRI volume		Wet muscle mass	
	RV (μL)	LV+S (μL)	RV (mg)	LV+S (mg)
Normoxic mice ($n = 6$)	24 ± 3	113 ± 4	27.2 ± 1.5	105 ± 8
Chronic hypoxic ($n = 5$)	31 ± 3*	91 ± 4*	47 ± 2.5*	119 ± 7

* $P < 0.05$ (analysis of variance test).

flip angle), an obvious benefit for high-resolution imaging. Until now, the only two publications that document black-blood imaging of mouse heart at 4.7 T showed the use of an additional module for magnetization preparation (6,8). In those studies, blood signal appeared less suppressed and the spatial resolution was lower than in the present work. Thus, the TrueFISP sequence proposed here affords high image quality in reasonable scan times (<1 h).

TrueFISP imaging of mouse heart at high field needs retrospective ECG gating, whereas no respiratory gating was necessary (24). This avoids the need for time-consuming preparation and makes it possible to choose a posteriori the number of reconstructed images per cycle. The choice depends on the heart rate of each animal and on the required SNR. Increasing the number of reconstructed image per cycle would require either a high number of repeated acquisitions (more than 48) or an interpolation method to fulfill each *k*-space volume.

As previously described (20), it was not possible to homogenize the magnetic field in order to generate artifact-free TrueFISP images, particularly in the heart. Therefore, multiple acquisitions with sum-of-square reconstruction were performed, thereby allowing the reconstruction of artifact-free 4D images. Of course, the acquisition of four sets of images limited the minimum total acquisition time. At higher field strengths, at least eight sets of images would have to be acquired in order to correct the banding artifact. Consequently, an additional technique like parallel imaging or partial *k*-space acquisition would be required to circumvent too long suppressed an acquisition time, which would not be compatible with in vivo imaging.

Altogether, the quality of the images presented shows that the proposed method is appropriate for 4D mouse heart imaging, particularly in terms of spatial resolution and blood signal suppression. Images are obtained in less than 1 h of scan time, a duration that can easily be reduced with an acceptable loss in spatial resolution.

This new technique, which efficiency has been demonstrated on control mice, also makes it possible to estimate cardiac anatomic modifications developed in mice exposed to 4-week chronic hypoxia. Indeed, pulmonary hypertension-induced right ventricular hypertrophy, which was previously documented in the literature by an increase in the right ventricle-to-heart mass ratio, can now be visually evaluated in mice and quantified with volume analysis segmentation. Even the slight reduction in left ventricular volume induced by right ventricular hypertrophy, with regard to the interdependence of the left and right ventricles in health and disease (25), can be evidenced in mouse heart. This technique therefore seems particularly adapted to describing more precisely the anatomic and functional changes occurring in numerous animal models of cardiac disease or during therapies.

The method can be easily implemented on standard MRI systems operating at 1.5 T or 3 T. The value of the method for the assessment of cardiac contractility in humans remains to be evaluated.

ACKNOWLEDGMENTS

Grant sponsors: Region Aquitaine, CNRS.

APPENDIX

$$M_{xy\_GEernst} = M_0 \sin\alpha_{opt} \frac{1-\exp(-TR/T_1)}{1-\exp^2(-TR/T_1)}$$

with

$$\cos\alpha_{opt} = \exp(-TR/T_1)$$

$$M_{xy\_TrueFISP} = M_0 \frac{1-\exp(-TR/T_1)\sin\alpha}{1-\exp(-TR/T_1)\cos\alpha - \exp(-TR/T2)(\exp(-TR/T1)-\cos\alpha)}$$

REFERENCES

1. Ruff J, Wiesmann F, Hiller KH, Voll S, von Kienlin M, Bauer WR, Rommel E, Neubauer S, Haase A. Magnetic resonance microimaging for noninvasive quantification of myocardial function and mass in the mouse. Magn Reson Med 1998;40:43–48.
2. Slawson SE, Roman BB, Williams DS, Koretsky AP. Cardiac MRI of the normal and hypertrophied mouse heart. Magn Reson Med 1998;39:980–987.
3. Wiesmann F, Ruff J, Hiller KH, Rommel E, Haase A, Neubauer S. Developmental changes of cardiac function and mass assessed with MRI in neonatal, juvenile, and adult mice. Am J Physiol Heart Circ Physiol 2000;278:H652–H657.
4. Wiesmann F, Ruff J, Engelhardt S, Hein L, Dienesch C, Leupold A, Illinger R, Frydrychowicz A, Hiller KH, Rommel E, Haase A, Lohse MJ, Neubauer S. Dobutamine-stress magnetic resonance microimaging in mice: acute changes of cardiac geometry and function in normal and failing murine hearts. Circ Res 2001;30:88:563–569.
5. Bishop J, Feintuch A, Bock NA, Nieman B, Dazai J, Davidson L, Henkelman RM. Retrospective gating for mouse cardiac MRI. Magn Reson Med 2006;55:472–477.

6. Feintuch A, Zhu Y, Bishop J, Davidson L, Dazai J, Bruneau BG, Henkelman RM. 4D cardiac MRI in the mouse. NMR Biomed 2007;20:360–365.
7. Bucholz E, Ghaghada K, Qi Y, Mukundan S, Johnson GA. Four-dimensional MR microscopy of the mouse heart using radial acquisition and liposomal gadolinium contrast agent. Magn Reson Med 2008;60:111–118.
8. Berr SS, Roy RJ, French BA, Yang Z, Gilson W, Kramer CM, Epstein FH. Black blood gradient echo cine magnetic resonance imaging of the mouse heart. Magn Reson Med 2005;53:1074–1079.
9. Edelman RR, Chien D, Kim D. Fast selective black blood MR imaging. Radiology 1991;181:655–660.
10. Mugler JP 3rd, Brookeman JR. The design of pulse sequences employing spatial presaturation for the suppression of flow artifacts. Magn Reson Med 1992;23:201–214.
11. Simonetti OP, Finn JP, White RD, Laub G, Henry DA. Black blood T2-weighted inversion-recovery MR imaging of the heart. Radiology 1996;199:49–57.
12. Croisille P, Guttman MA, Atalar E, McVeigh ER, Zerhouni EA. Precision of myocardial contour estimation from tagged MR images with a "black-blood" technique. Acad Radiol 1998;5:93–100.
13. Sirol M, Itskovich VV, Mani V, Aguinaldo JG, Fallon JT, Misselwitz B, Weinmann HJ, Fuster V, Toussaint JF, Fayad ZA. Lipid-rich atherosclerotic plaques detected by gadofluorine-enhanced in vivo magnetic resonance imaging. Circulation 2004;109:2890–2896.
14. Oppelt A, Graumann R, Barfu H, Fischer H, Hartl W, Schajor W. FISP: a new fast MRI sequence. Electromedica 1986;54:15–18.
15. Wieben O, Francois C, Reeder SB. Cardiac MRI of ischemic heart disease at 3 T: potential and challenges [review]. Eur J Radiol 2008;65:15–28.
16. Jahnke C, Paetsch I, Gebker R, Bornstedt A, Fleck E, Nagel E. Accelerated 4D dobutamine stress MR imaging with k-t BLAST: feasibility and diagnostic performance. Radiology 2006;241:718–728.
17. Rettmann DW, Saranathan M, Wu KC, Azevedo CF, Bluemke DA, Foo TK. High temporal resolution breathheld 3D FIESTA CINE imaging: validation of ventricular function in patients with chronic myocardial infarction. J Magn Reson Imaging 2007;25:1141–1146.
18. Greil GF, Germann S, Kozerke S, Baltes C, Tsao J, Urschitz MS, Seeger A, Tangcharoen T, Bialkowsky A, Miller S, Sieverding L. Assessment of left ventricular volumes and mass with fast 3D cine steady-state free precession k-t space broad-use linear acquisition speed-up technique (k-t BLAST). J Magn Reson Imaging 2008;27:510–515.
19. Bangerter NK, Hargreaves BA, Vasanawala SS, Pauly JM, Gold GE, Nishimura DG. Analysis of multiple-acquisition SSFP. Magn Reson Med 2004;51:1038–1047.
20. Miraux S, Massot P, Ribot EJ, Franconi JM, Thiaudiere E. 3D TrueFISP imaging of mouse brain at 4.7T and 9.4T. J Magn Reson Imaging 2008;28:497–503.
21. Calmettes G, Deschodt-Arsac V, Thiaudiere E, Muller B, Diolez P. Modular control analysis (MoCA) of the effects of chronic hypoxia on mouse heart. Am J Physiol Regul Integr Comp Physiol 2008;295:R1891–R1897.
22. Gilson WD, Yang Z, French BA, Epstein FH. Measurement of myocardial mechanics in mice before and after infarction using multislice displacement-encoded MRI with 3D motion encoding. Am J Physiol Heart Circ Physiol 2005;288:H1491–H1497.
23. Kober F, Iltis I, Cozzone PJ, Bernard M. Myocardial blood flow mapping in mice using high-resolution spin labeling magnetic resonance imaging: influence of ketamine/xylazine and isoflurane anesthesia. Magn Reson Med 2005;53:601–606.
24. Ruff J, Wiesmann F, Lanz T, Haase A. Magnetic resonance imaging of coronary arteries and heart valves in a living mouse: techniques and preliminary results. J Magn Reson 2000;146:290–296.
25. Clyne CA, Alpert JS, Benotti JR. Interdependence of the left and right ventricles in health and disease [review]. Am Heart J 1989;117:1366–1373.